Fine particulate emission control by optimizing process parameters of an electrostatic precipitator

S. M. E HAQUE[1], M. G. RASUL[2*], M. M. K KHAN[2]

[1]Process Engineering & Light Metals (PELM) Centre
Faculty of Sciences, Engineering and Health
CQUniversity
Gladstone, Queensland 4680
AUSTRALIA
[2]College of Engineering and the Built Environment
Faculty of Sciences, Engineering and Health
CQUniversity
Rockhampton, Queensland 4702
AUSTRALIA

*Corresponding author: Email: m.rasul@cqu.edu.au

Abstract: - This paper presents a numerical model of a wire-plate electrostatic precipitator (ESP) for analysing its fine particulate collection behaviour. Computational fluid dynamics (CFD) code FLUENT is used to solve the two-dimensional Navier–Stokes equations for the gas flow and the realizable k-ε turbulence model for the turbulence. The effect of electric field has been captured by adding a source term in the momentum equation. This additional source term is obtained by solving a coupled system of the electric field and charge transport equations. The particle phase is simulated by using Discrete Phase Model (DPM). The results of the simulation revealed that the particle collection and its movement depend not only on the size of the particle but also on the velocity of the gas flow and the electric potential applied at the discharge electrodes.

Key-Words: - ESP; CFD; Fine particulate; DPM; Electric potential

1 INTRODUCTION

Electrostatic precipitators (ESP) are the most widely used devices that are capable of controlling particulate emission effectively from power plants and other process industries. A typical ESP consists of a series of parallel collection electrodes (CE), oriented along the direction of the flue gas flow. A number of thin discharge electrodes (DE) are suspended vertically between these plates. The precipitation process involves charging particles of the flue gas by applying high negative voltage to the discharge electrodes and driving the charged particles towards the grounded CE by the electric field produced. The negligible change of the electric field in the vertical direction justifies a two-dimensional modelling approach of this study.

There is a limited research found in the literature on ESP simulation. Most researches [1 - 4] simplified their model by creating a single DE ESP configuration. Single wire model may not be capable of capturing the wake of the wires properly and it can not be assumed that the particle motions will be repeated in the gas flow direction. Hence three wires have been taken into consideration for the development of a representative numerical model of ESP. It is noted that only a limited research [5 - 7] is found in the literature where three wires have been considered for modelling an ESP channel.

The present study takes a comprehensive approach for predicting the motion of gas, ions and particles inside an ESP channel. The model was verified elsewhere [8] with the available literature data. The result of the simulation showed that the collection of fine particulate can be improved by optimizing process parameters of an ESP.

2 GEOMETRY CONFIGURATIONS

Two collection electrodes and three discharge electrodes were considered for creating the geometry of an ESP channel. Due to the symmetry of the geometry only half a channel was modelled in this study as is shown in Fig. 1. The Fluent Inc. geometry and mesh generation software

"GAMBIT" was used as a pre-processor for geometry development and fluid domain discretization purposes. The computational mesh consists of 15000 cells and is shown in Fig. 2. It also shows the boundary conditions that were used in this study for solving the problem. Unstructured quadrilateral/hexahedral elements have been chosen for meshing the 2D ESP model as they permit a much larger aspect ratio than triangular/tetrahedral cells for a relatively simple geometry [9].

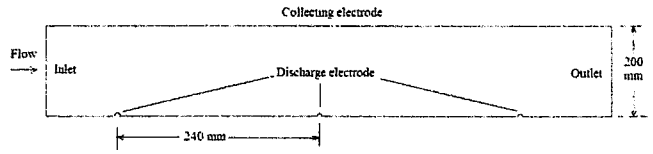

Fig. 1: 2D geometry configuration

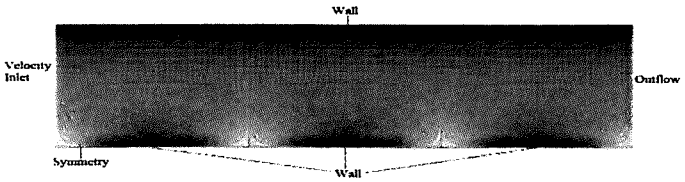

Fig. 2: Computational mesh

3 GOVERNING EQUATIONS

The two-dimensional Navier–Stokes equations were solved to model the gas flow. An additional source term is added to the gas flow equation to introduce the electric field inside the ESP channel. Lagrangian Discrete Phase Model (DPM) was used to calculate and monitor particle trajectories.

3.1 Gas Dynamics

The air inside the lab ESP was treated as incompressible Newtonian fluid due to the small pressure drop across it. The flow was assumed to be steady and can be described by the conservation of mass equation: The air inside the ESP is treated as incompressible Newtonian fluid due to the small pressure drop across the ESP. The flow can be described by the Conservation of mass equation:

$$\frac{\partial \rho}{\partial t} + \vec{\nabla} \cdot (\rho \vec{V}) = 0 \quad (1)$$

and the Momentum equation known as Navier-Stokes equation:

$$\frac{\partial \vec{V}}{\partial t} + \vec{V}.\vec{\nabla}\vec{V} = -\frac{\vec{\nabla} p}{\rho} + \nu \vec{\nabla}^2 \vec{V} + S \quad (2)$$

Where ρ is the fluid density (kg/m^3), v is the kinemetic viscosity (m^2/s) of the fluid, p is the fluid pressure (Pa) and $\vec{V}$ is the fluid velocity (m/s). S is the source term, which expresses the momentum force (N/m^2) on the gas flow due to the electric field and can be expressed as [5],

$$S = \rho_{ion} \vec{E} \quad (3)$$

Here ρ_{ion} is the ion charge density (C/m^3) and $\vec{E}$ is the electric field intensity (V/m).

The realizable $k-\varepsilon$ model is used in this study to capture the turbulent behaviour of flow inside the ESP.

3.2 Electrostatic Field

The electric field intensity $\vec{E}$ inside the ESP can be described by the Gauss's law equation [10]),

$$\nabla.\vec{E} = \frac{\rho_{ion}}{\varepsilon_0} \quad (4)$$

Where

$$\vec{E} = -\nabla \phi \quad (5)$$

Combining Equations (4) and (5) gives the well known Poisson equation which is defined as

$$\nabla^2 \phi = -\frac{\rho_{ion}}{\varepsilon_0} \quad (6)$$

Where $\vec{E}$ is the electric field intensity (V/m), ϕ is the electric potential (Volt) and ε_0 is the permittivity of the free space. Under stationary conditions, the electrical flux density is divergence-free and can be written as [11],

$$\nabla.\vec{J} = 0 \quad (7)$$

Here $\vec{J}$ is the density of ionic current.

Assuming ion diffusion is of negligible importance compared to conduction [1, 11], $\vec{J}$ can be expressed as,

$$\vec{J} = \rho_{ion} b_{ion} \vec{E} \quad (8)$$

Here b_{ion} is the ion mobility.

Combining Equation (7) and (8) gives the following expression,

$$\nabla.(\rho_{ion} b_{ion} \nabla \phi) = 0 \quad (9)$$

With the appropriate boundary conditions and a solution method, two transport variables ϕ and ρ_{ion} were numerically calculated.

3.3 Particle Dynamics

FLUENT predicts the trajectory of a discrete phase particle by integrating the force balance on the particle, which is written in a Lagrangian reference frame. This force balance equates the particle inertia with the forces acting on the particle, and can be written as [9],

$$\frac{du_{p,i}}{dt} = F_D(u_i - u_{p,i}) + \frac{g_i(\rho_p - \rho)}{\rho_p} + F_i \quad (10)$$

Where ρ_p and $u_{p,i}$ denote particle density and velocity respectively. $F_D(\vec{u}_i - \vec{u}_{p,i})$ is the drag force per unit particle mass and F_i corresponds to external forces exerted on the particle that, in the present study, are the electrostatic forces [12],

$$F_i = \frac{E_i q_p}{m_p} \quad (11)$$

Where, E_i is the electric field components [V/m] and m_p is the particle mass [kg]. The particle charge, q_p, determines the Coulomb force, which is exerted on the particle. It is calculated in the Lagrangian framework, as the particle moves through the gas by the following expression,

$$\frac{dq_p}{dt} = \frac{1}{\tau q_{\max}}(q_{\max} - q_p) \quad (12)$$

Here, τ is the time taken for the particle to reach half the saturation charge [s] and is defined as,

$$\tau = \frac{4\varepsilon_0}{\rho_{ion} b_{ion}} \quad (13)$$

Where b_{ion} is the ion mobility = 0.00022 (for air ions) [$m^2C/J/s$] = [$m^2/V/s$].

q_{max} is the saturation charge by the local electric field at the particle location and is expressed as,

$$q_{\max} = q_{sat} = \frac{3\pi\varepsilon_o\varepsilon_r E d_p^2}{\varepsilon_r + 2} \quad (14)$$

Where ε_o is the permittivity of free space and is equal to $8.854X10^{-12}$ [$C^2/N/m^2$] and ε_r is the relative permittivity of the gas (or dielectric constant of the gas) which for air is 1.000590.

4 BOUNDARY CONDITIONS

The geometry developed by GAMBIT is exported to FLUENT solver to specify the flow properties, solve the problems and analyse the results. The finite volume methods were used to discretise the partial differential equations of the model using the SIMPLEC method for pressure–velocity coupling and the second order upwind scheme to interpolate the variables on the surface of the control volume. The segregated solution algorithm is selected to solve the governing equations sequentially. Non-equilibrium wall functions were applied to bridge the viscosity-affected region between the wall and the fully-turbulent region.

The electric potential on the collection plates is zero whereas at the discharge electrode surface the value is 70 (kV). The charge density ρ_0 at the discharge electrode can be approximately calculated by [13],

$$\rho_0 = -\frac{\varepsilon(E - E_0)}{ds} \quad (15)$$

Where E is the field strength in the cell adjacent to the emitting electrode, ds is the distance between the cell and the electrode surface. The corona onset field E_0 along the corona-emitting surface is assumed constant, and it can be obtained according to Peek's law [14],

$$E_o = E_{Peek} = 3.1X10^6\delta(C_1 + C_2/\sqrt{\delta r}) \quad (16)$$

Where E_{Peek} is the ion current threshold value for an electrode of radius r and C_1 = 1 V/m and C_2 = .031 V/$\sqrt{}$m in air of relative density δ with respect to the normal temperature and pressure conditions.

A number of subroutines were written and compiled by using User-Defined-Functions (UDF) compatible with FLUENT. The UDFs are then linked to the standard fluid model to solve the Poisson's equation and the charge density equation. The operating gas was ambient air while the particles were assumed to be ash with density equal to 600 kg/m^3. Turbulent intensity at the inlet was 5%. Boundary conditions used to solve this problem are summarised in Table 1.

Table 1: Boundary conditions applied to the ESP model

	Gas dynamics	Electric potential (kV)	Ion charge density C/m^3	Particle dynamics
Velocity Inlet	$u_x = 1.0m/s$ $u_y = 0.0m/s$	$\nabla\phi = 0$	$\nabla\rho_{ion}$ = 0	$u_{p_x} = 1.0m/s$ $u_{p_y} = 0.0m/s$ Escape
Outflow	Mass conservation	$\nabla\phi = 0$	$\nabla\rho_{ion}$ = 0	Escape
Wall-Collecting electrode	No slip	$\Phi = 0$	$\nabla\rho_{ion}$ = 0	Trap
Wall-Discharge electrode	No slip	Φ = 60, 70, 80, 90	Peek law	Reflect

5 RESULTS AND DISCUSSION

5.1 Influence of Particle Diameter on Collection Efficiency of an ESP

It is important to study the influence of particle diameter on the particle collection since the size of particles in an ESP system varies greatly from micrometre size to millimetre. Particle diameter is taken directly into account in the drag force and particle charge relationship and, thus, influences the collection of the particle. The effect of particle diameters on particle collection is shown in Fig. 3 where 500 particles with a size range from 1μm to 141 μm were injected from the inlet surface with the velocity of 1 m/s. Rosin-Rammler distribution was adopted with the mean particle diameter of 18.11 μm. The electric potential at the boundaries of the discharge electrodes is set at 70 kV.

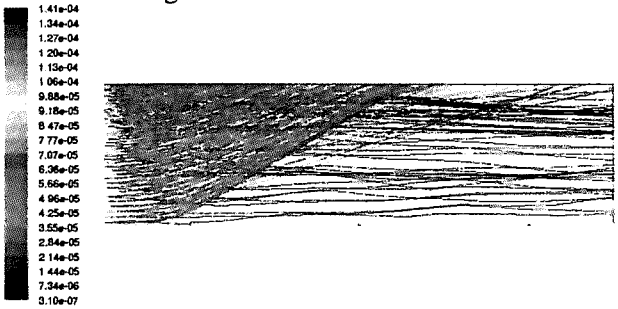

Fig. 3: Particle trajectories coloured by particle diameter
(Gas velocity 1m/s, Electric potential 70 kV)

The simulation shows that the current operating condition will not be able to capture the particles with a size less than 5 μm effectively as most of them have escaped from the collection area. The collection efficiency was calculated by dividing the number of particles collected inside the ESP with the number of particles injected. The result of the simulation shows that the collection efficiency of the ESP channel decreases with the decrease in particle size. The collection efficiencies are 30% for particles with a size of 2.5 μm and 18% for 1 μm sized particles. Fig. 4 presents the trajectory of the particles with a size of 1 μm where 9 particles were collected after injecting 50 particles inside the ESP.

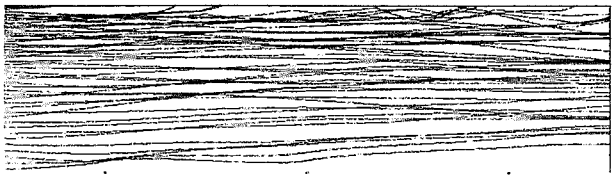

Fig. 4: Trajectory of particles (Size 1 μm, Gas velocity 1m/s and electric potential 70 kV)

5.2 Influence of Gas Velocity on Collection Efficiency of ESP

The influence of gas velocity on particle collection was studied. The 3D ESP model of this study revealed that the velocity is not uniformly distributed across the collection chamber. The average gas velocity inside the collection chamber of an ESP varies from 0.5m/s to 2 m/s. However, it is crucial to optimize the flow for improving the collection of particles. The flow stream with high velocity leaves the collection chamber with poor particle collection. The particles need sufficient treatment time to get charged and collected inside an ESP. The collection efficiencies for all sizes of particles have significantly dropped while the velocity of the flow at the inlet surface is increased to 1.5 m/s. The efficiency dropped to 18% for the particles with a size of 2.5 μm and 10% for 1 μm sized particles. Fig. 5 shows the trajectory of the particles with a size of 1 μm where only 5 particles were collected after injecting 50 particles inside the ESP.

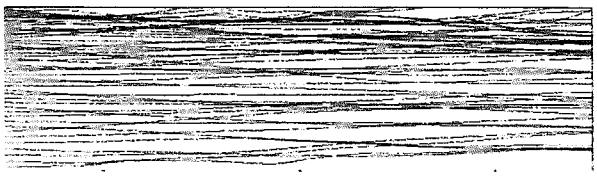

Fig. 5: Trajectory of particles (Size 1 μm, Gas velocity 1.5 m/s and electric potential 70 kV)

The simulated results show significant improvement in the collection of fine particles while the velocity of the flow at the inlet surface is reduced to 0.5 m/s. The collection efficiencies for the 2.5 μm and 1 μm sized particles have increased to 42% and 24%. Fig. 6 shows the trajectory of the particles of the size of 1 μm where 12 particles where captured after injecting 50 particles inside the ESP.

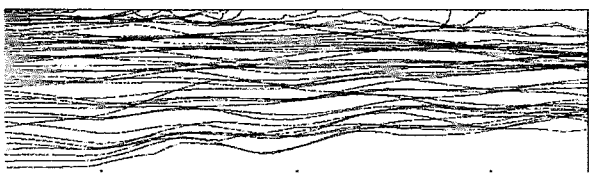

Fig. 6: Trajectory of particles (Size 1 μm, Gas velocity 0.5 m/s and electric potential 70 kV)

5.3 Influence of Electric Potential on Collection Efficiency of ESP

The particle collection inside the ESP greatly depends on the electrostatic force of the ESP system. The electrostatic force, which is generated after applying electric potential on the discharge

electrodes are strongly related to the movement of the particles. A range from 60 kV to 90 kV electric potential is applied to the discharge electrode to study its influence on the particle collection inside the ESP. The results of the simulation revealed that the particle collection efficiency is reduced with the decreased electric potential at the surface of the discharge electrodes. The collection efficiencies are 20% and 12% for particles with a size of 2.5 μm and 1 μm respectively. Fig. 7 presents the trajectory of the particles of the size of 1 μm where only 6 particles were capture after injecting 50 particles inside the ESP.

Fig. 7: Trajectory of particles (Size 1 μm, Gas velocity 1m/s and electric potential 60 kV)

The collection of particles could be improved after increasing the electric potential at the discharge electrodes. The collection efficiencies are 34% and 20% for the particles with a size of 2.5 μm and 1 μm respectively while the applied electric potential at the discharge electrodes is 80 kV. Fig. 8 shows the trajectory of the particles with the size of 1 μm where 10 out of 50 particles were collected.

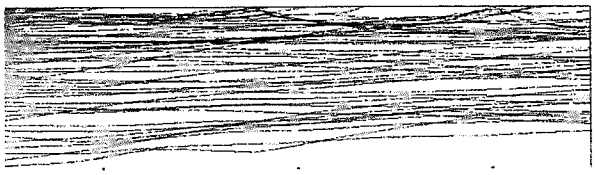

Fig. 8: Trajectory of particles (Size 1 μm, Gas velocity 1m/s and electric potential 80 kV)

No further improvements on particulate collection were observed after increasing the electric potential to 90 kV.

5.4 Improvement of collection efficiency by applying optimized gas velocity and electric potential

The collection efficiency of the fine particulate was found to be improved in Fig. 10 after setting the optimized gas velocity (0.5 m/s) at the inlet boundary and an increase of electric potential at the discharge electrode from 70 kV to 80 kV.

(a) Trajectory of particles
(Size 2.5 μm, Injected-50, Collected- 24)

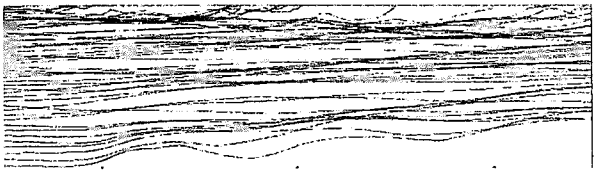

(b) Trajectory of particles
(Size 1 μm, Injected-50, Collected- 14)
Fig. 9: Particle trajectories (Gas velocity 0.5 m/s and electric potential 80 kV)

The simulated results show significant improvement of the collection of particles while the gas velocity was 0.5 m/s and the electric potential was 80 kV. The collection efficiencies for the 2.5 μm and 1 μm sized particles are increased to 48% and 28%.

Fig. 10 shows the trajectory of the particles while the flow velocity is maintained 0.5 m/s at the inlet boundary but the electric potential is increased to 90 kV.

(a) Trajectory of particles
(Size 2.5 μm, Injected-50, Collected- 29)

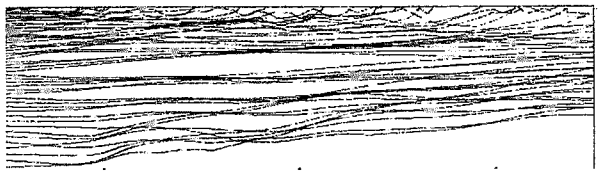

(b) Trajectory of particles
(Size 1.0 μm, Injected-50, Collected- 18)
Fig. 10: Particle trajectories (Gas velocity 0.5 m/s and electric potential 90 kV)

A further increase in electric potential is found to create improved collection efficiency of the ESP. The collection efficiency is increased to 58% for the particles with a size of 2.5 μm and 36% for 1 μm sized particles.

6 CONCLUSION

A two dimensional ESP channel consisting of three discharge electrodes was modelled. The electrostatic field was solved through writing and compiling a number of subroutines and linking them with the standard version of FLUENT 6.2 software. A Discrete Particulate Phase (DPM) model was used for calculating particle trajectories. The study revealed that particles with a size of less than 2.5 μm are found to be difficult to capture as most of them escaped from the collection chamber, whereas 100% collection could be achieved for the large particles (>18 μm). This is because the higher charge of the large particles forces them towards the collection electrode for deposition. The large particle acquires more charge than a small one due to its larger surface area; the larger the diameter of the particle, the higher is the charge and the more efficient is the particle collection. However, it is evident from the simulated results that the increased electric potential cannot improve the collection of fine particles unless the flow velocity is adjusted and optimized. The optimized flow velocity results in fine particles to spend more time inside the collection chamber and so collect a sufficient charge, which is crucial for their movement towards the collection electrodes.

References:

[1] Lami, E., Mattachini, F., Gallimberti, I., Turri, R. and Tromboni, U., A numerical procedure for computing the voltage-current characteristics in electrostatic precipitator configurations, Journal of Electrostatics, 34, 1995, 385 – 399.

[2] Zhao, L., Cruz, E. Dela., Adamiak, K., Berezin, A. A., Chang, J.S. (2006). A numerical model of a wire-plate electrostatic precipitator under electrohydrodynamic flow conditions, The 10th International conference on electrostatic precipitator, Australia. 2006.

[3] Park, Seok. Joo & Kim, Sang. Soo., Effects of electrohydrodynamic flow and turbulent diffusion on collection efficiency of an electrostatic precipitator with cavity walls, Aerosol Science and Technology, 37, 2003, 574–586.

[4] Anagnostopoulos, J. & Bergeles, J., Corona discharge simulation in wire-duct electrostatic precipitator, Journal of Electrostatics 54, 2002, 129–147.

[5] Choi, B.S., and Fletcher, C.A.J, Turbulent particle dispersion in an electrostatic precipitator, Applied mathematical modeling, 22, 1998, 1009 – 1021.

[6] Nikas, K.S.P., Varonos, A.A. and Bergeles, G.C., Numerical simulation of the flow and the collection mechanisms inside a laboratory scale electrostatic precipitator, Journal of electrostatics, 63, 2005, 423 – 443.

[7] Egli, Walter., Kogelschatz, Ulrich., Gerteisen, Edgar. A. and Gruber, Ralf., 3D computation of corona, ion induced secondary flows and particle motion in technical ESP configurations, Journal of electrostatic, 40&41, 1997, 425 – 430.

[8] Haque, Shah. M. E., Rasul, M. G., Khan, M. M. K., Deev, A.V. and Subaschandar, N. A Numerical Model of Particle Motion in an Electrostatic Precipitator, *Proceedings of the 16th Australasian Fluid Mechanics Conference, CD-ROM, pp. 1050-1054*, Crowne Plaza, Gold Coast, 3-7 December 2007, Australia.

[9] Fluent Inc. (2005). Fluent 6.2 User's Guide.

[10] Kallio, Gregory A. and Stock, David E., Computation of electrical conditions inside wire-duct electrostatic precipitators using a combined finite-element, finite-differnece technique, Journal of Applied Physics, 59 (6), 1986, 1799 – 1806.

[11] Poppner, Marc., Sonnenschin, Rainer. and Meyer, Jorg., Electric fields coupled with ion space charge. Part 2: computation, Journal of electrostatics, 63, 2005, 781 – 787.

[12] A.A.Varonos, J.S.Anagnostopoulos, G.C.Bergeles, Prediction of the cleaning efficiency of an electrostatic precipitator, Journal of Electrostatics, Vol. 55, 2002, pp. 111 – 133

[13] Ye, Q. and Domnick, J., On the simulation of space charge in electrostatic powder coating with a corona spray gun, Powder technology, 135-136, 2003, 250 – 260.

[14] Peek, F.W., Determination Phenomena in High Voltage Engineering, McGraw-Hill, New York, 1929, 52–80.